Experimental Study on U-Beam Separator Device for Separating Solids from Gases

Rémy Aubry, Matthieu Debal, Stéphane Aubert, Yann Rogaume

energies

MDPI

Article

Experimental Study on U-Beam Separator Device for Separating Solids from Gases

Rémy Aubry *, Matthieu Debal, Stéphane Aubert and Yann Rogaume

INRAE, LERMAB, ERBE, Université de Lorraine, F-88000 Epinal, France
* Correspondence: remy.aubry@univ-lorraine.fr; Tel.: +33-661-73-3339

Abstract: The inertial separator, developed for fluidized beds, is a key component for optimizing large installations that separate solids from gases. Despite industrial interest and numerous patents, few studies have been conducted on this subject. In this paper, the geometric arrangement conditions were studied and evaluated. The efficiency of separating solids from gas depends on several factors, such as the granulometry, density, particle size distribution, velocity, humidity, and temperature of the system. For the mid-range of fluidized bed boilers (1–20 MWth), the experimental study selected all data to be in the same condition as the industrial technology. The global performance of the system can be increased by 15% by selecting a better combination of the U-beam. Three rows of U-beams are a good compromise between performance and cost for high Reynolds numbers, while only two rows seem to be enough for lower Reynolds numbers.

Keywords: U-beam separator; particulate matter; particle size distribution; inertial impaction; particle trapping

Citation: Aubry, R.; Debal, M.; Aubert, S.; Rogaume, Y. Experimental Study on U-Beam Separator Device for Separating Solids from Gases. *Energies* **2023**, *16*, 4975. https://doi.org/10.3390/en16134975

Academic Editor: Vladislav A. Sadykov

Received: 5 May 2023
Revised: 23 June 2023
Accepted: 24 June 2023
Published: 27 June 2023

1. Introduction

Because of global warming, mentioned by the expert of the IPCC [1], emissions from human activities should be reduced in order to mitigate the rise in temperatures. Every country in the world has been urged to reduce their impact on the environment by implementing green policies.

Since 1990, the French government has created a special agency to tackle these problems. ADEME, the French agency for energy and waste, has been developing "renewable heating funds" and "R&D programs" for many years to help with the development of industrial technologies for district heating, specifically for low and medium ranges of power (1 to 20 MWth) using renewable fuel such as wood or RDF (Refuse-Derived Fuels).

The technology used for biomass boilers for this range of power are mainly grate grids [2]. In these boilers, pellets and woodchips are easily burnt on a standard grate grid. However, due to the intensification of biomass development [3], new fuels need to be considered. As shown by [4], new fuels comparable to standard fuels, such as RDF or challenging biomasses, could be considered, but they present some challenges (corrosion with ashes [5]), particularly for conventional grate grid furnaces. Some studies have evaluated the ability to mix the product during combustion to push the technological limits of the grate [6]. The best available technology for this type of mixed fuel remains the fluidized bed boiler due to the mixing of the material in the bed.

Fluidized beds are designed with a mechanical dust collector (MDC), i.e., the cyclone. This is the most standard and economic system to separate particles from gas, and obviously, the most studied equipment [7–11]. Indeed, in industrial systems, there are three main reasons to separate solids from gases: to minimize emissions for the environment [12], to protect the downstream part of the installation, and to avoid unwanted reactions between the gas and solid. For fluidized bed boilers, the goal is to have fewer particles to clean in the flue gas before the final treatment, such as a bag filter or an electrostatic

precipitator. However, the temperature inside the combustion room is very high (around 1000 °C, according to [13]). In that way, the cost of cyclone technology is more expensive than standard MDC [14,15]. During the golden age of the development of fluidized bed boilers [16], industrial companies tried to find a more economic system. They developed several patents on an inertial impaction technology during the nineties. This technology uses U-shaped impactors, called U-beams, as shown in Figure 1, in staggered rows across a stream of dust-laden air from the combustion chamber.

The first two patents proposed the baffle to separate particles from the flow [17] and the solution of the U-shape [18]. Then, the inventors worked on a cooling system to save and use thermal energy from the flue gas [19] for steam use, [20] for heat exchange, [21,22] for the shape of the beam. The last two patents proposed an integrated beam and cooling system, which is more complicated to industrialize due to the shape and welds of the beam.

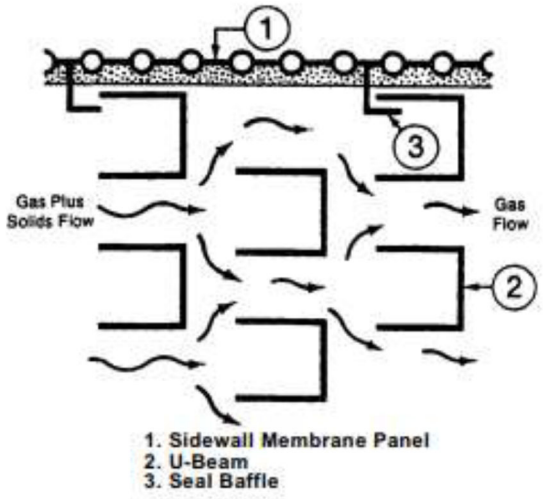

Figure 1. Overview of the U-beam distribution extracted from [18].

Thanks to all these developments, the inertial impaction device is able to be used in a global circulating fluidized bed (CFB) using economical raw materials [23] and technology to enhance efficiency. However, after being impacted, the particles could return to the flow, which is known as the "flying away" phenomenon. To avoid this, [24] developed a drainage system that includes six rows of beams.

The efficiency and pressure drop were evaluated and were found to be comparable for inertial impaction against the cyclone [25].

Reference [14] compares both solutions, and despite their comparable efficiency, hot cyclones have a higher cost, a higher risk of wear [26], a larger size due to temperature, and a higher pressure drop estimated to be equal to 2 kPa. However, [27,28] do not agree on the latter point. A previous study [29] suggested that the pressure drop is directly proportional to the dust concentration, which could explain the difference in the two studies. Nevertheless, the advantages of inertial impaction have been further developed to increase the thermal performance of the system while finding a standard material and reducing manufacturing costs. New developments include the clever addition of an edge at the end of the beam to prevent particle bouncing [14,30].

Finally, a two-stage solids separation system could be used in addition to the cooling system to reduce the quantity of fine solid fractions to be treated by the final filter and to keep the larger particles inside the boiler [15].

Fluidized bed technology for boilers is the best option for burning Solid Recovery Fuels (SRF) [26] and other biomass products [27], even for mid-range thermal power. To enhance the efficiency of biomass boilers in using various fuels, a project called "POLYBIOM" [28] was launched.

In this project, a fluidized bed boiler was developed with a medium speed of fluidization (3.5 $m \cdot s^{-1}$) [29,30]. Unlike grate boilers, the design and use of fluidized bed boilers present some additional constraints. The agglomeration of the bed is the biggest concern due to the risk of defluidization [31].

To prevent this problem and maintain a low temperature in the bed (below 800 °C) [32], two combustion zones were created to divide the fluidized bed into two "rooms." Both rooms have distinct combustion functions. An inertial separator, the U-beam, is located between the two rooms to prevent larger particles from passing through and to increase overall efficiency while reducing wear on the heat exchanger [33]. The heat transfer coefficient from the particles to the impact separators has been evaluated by [34], which suggests that the lowest possible temperature should be used to reduce thermal stresses in the impactors.

Simulations were carried out to model particle-containing flows. Even though the models are progressing, as the authors attest [35,36], the simulations do not cover the entire particle size distribution [37].

In this paper, the traditional U-beam separator is studied using experimental methods. The study evaluates the efficiency of the U-beam system's geometry for disposing of a mixture of air loaded with very fine particles. The impact of the geometry and initial conditions is also evaluated.

2. Materials and Methods

2.1. Geometry of the Equipment

Experiments were conducted in a building with a standard air temperature and a control air temperature. Figure 2 shows a side view of the device as installed, along with a list of the equipment and their roles. The device is designed to replicate the operation of a fluidized bed.

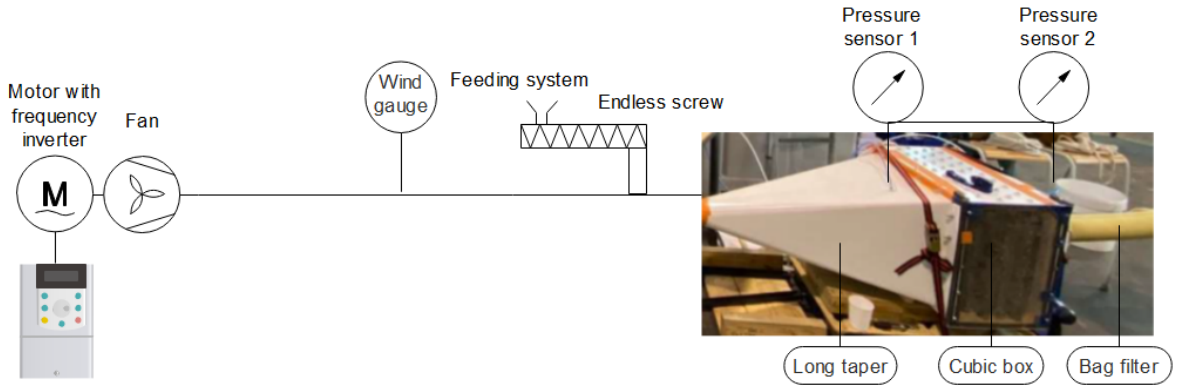

Figure 2. Overview of the system (pictures and scheme).

A fan controlled by a motor with a frequency converter produces the air flow at a variable flow rate, allowing the velocity (v) to be changed. The speed is measured using an anemometer (wind gauge) placed 1250 mm from the fan, which can measure velocities up to 40 $m \cdot s^{-1}$, corresponding to the common velocities in the U-beam zone of a fluidized bed.

A feeding system uses an endless screw to discharge sawdust into the PVC pipe, with a precision scale continuously measuring the mass introduced into the system. The sawdust is mixed with air before it reaches the U-beam.

A long taper is used for the inlet and a shorter taper for the outlet (not shown in Figure 2) to stabilize the flow of air and particles. The cubic box containing the U-beams can be reconfigured as needed. One pressure sensor measures the inlet pressure of the flow, while another measures the pressure at the outlet. These sensors are placed to measure only the pressure drop due to the U-beams. At the end of the system, a bag filter is installed to collect all particles and protect the testing room.

A plexiglass wall is used to visualize the areas where the particles deposit during testing and to facilitate cleaning of the room after each test (see Figure 2).

2.2. Geometry of U-Beam

As mentioned in Chapter 1, the separation beam should be as simple as possible and made of a common raw material. Therefore, a U-beam in structural steel was selected for the experiment. The following dimensions are shown in Figure 3, which correspond to a classical UPN profile (thickness $a = 5$ mm; width $b = 20$ mm; length $c = 40$ mm; space between two beams $d = c = 40$ mm; space between two rows $e = b = 20$ mm). Based on previous experimental studies [14,38], the arrangement of the U-beams was set up as shown in Figure 3, without a cover. A steel wall should be visible from the particle side.

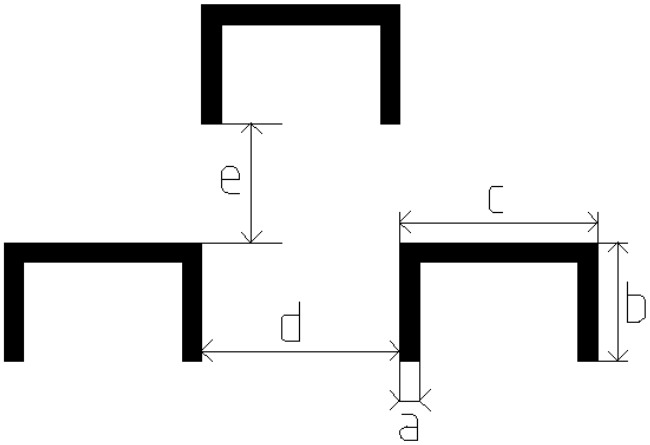

Figure 3. Dimensions (mm) of the U-beam.

2.3. Geometry of the Box

The above view of the system is presented in Figure 4. U-beams are placed into the "cubic box", screwed to the upper plate, and sealed. The cubic box is composed of six rows: three rows of eight beams and three rows of nine beams, to allow the maximum possibility for experience. The rows are arranged in staggered position according to Figure 3 with $g = 60$ mm and $f = 60$ mm.

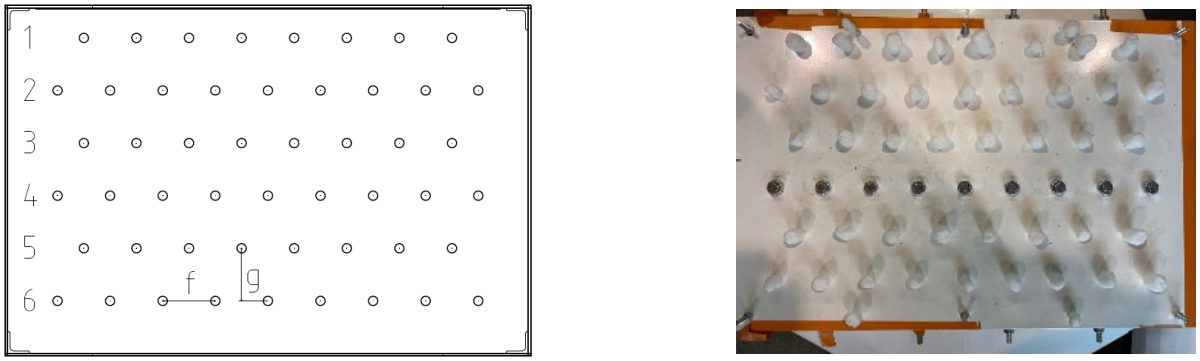

Figure 4. Overall system of the U-beam—scheme and picture with one row installed (top view).

All holes are plugged, for sealing purposes, except holes used for the configuration tested as seen in Figures 4 and 5. The number of the rows are written in Figure 4.

Figure 5. Overall system of the U-beam side view with three rows installed.

Figure 4 presents a top view of the cubic box, and Figure 5 shows a side view with three rows already installed. In Figure 4, the row numbers are indicated to check the influence of the position of the row during tests. The inside of the box is visible through a transparent plate. The following configurations were tested:

- without U-beam;
- with one row installed;
- with two rows installed at different positions in the system and with a variable space between the rows;
- with three rows installed at different positions in the system and with a variable space between the rows;
- with four rows.

Velocity, granulometry, and geometry of the arrangement were evaluated for the U-beam separator device in comparison to the empty one. An empty test was conducted to evaluate the deposition due to the form of the system and the mass of particles.

During the experimental measurements, precautions should be taken to prevent particulate matter from flying away. At the bottom of the system, wooden spacers or plastic foam were added to block the flow of the mixtures. In a fluidized bed, the particles collected by the U-beams will fall through a siphon.

2.4. Granulometry

The goal of the study is to show the system's ability to stop ash particles from combustion. According to [39,40], the size of the ash is divided into two size groups: fine particles with an average diameter of 0.015 µm, which are reactive, and large particles up to 100 µm in diameter, which are inert. For the experimentation, only large particles were considered because the fine particles would have reacted inside the rooms in the burner. Thus, in this studies, three types of particles were used and all of them were higher than 0.212 mm.

The particles used during the tests were sawdust (fine, medium, and coarse). The granulometry is presented in Figure 6. The histogram shows the mass distribution for all three sawdust types, and the curve represents the cumulative mass.

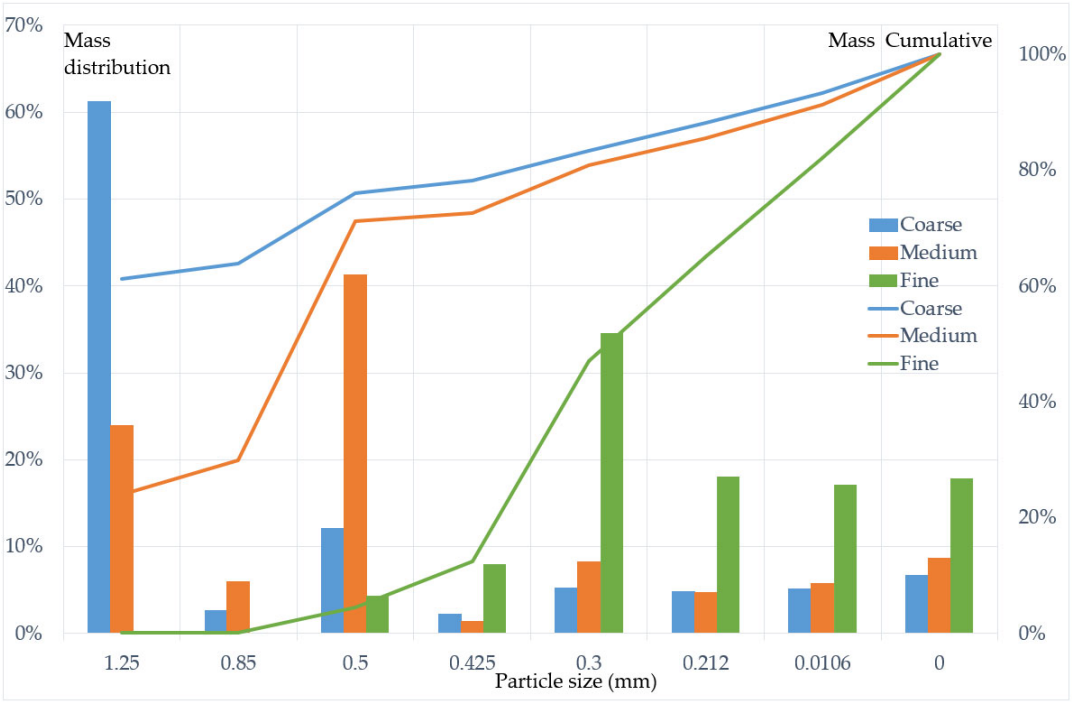

Figure 6. Granulometry of the coarse, medium, and fine sawdust (mm).

The medium and fine particles had a distribution similar to the one used by [25].

The average sizes of coarse particles were equal to 1.25 mm, 0.5 mm for medium, and 0.3 mm for fine.

2.5. Velocity

During the beginning of the test, different values of velocities were tested and two of them, Table 1, in turbulent mode were selected.

$$Re = \frac{\rho \times v \times D}{\mu} \quad (1)$$

with Re, Reynolds number; ρ, density (kg·m^{-3}); μ, dynamic viscosity; D, inner diameter; v, for the velocity.

Table 1. Reynolds number for both speed tests.

	ρ	v(m·s^{-1})	D (mm)	μ	Re
Test 1	1.204	18.48	94	1.8×10^{-5}	1.16×10^{5}
Test 2	1.204	34.42	94	1.8×10^{-5}	2.16×10^{5}

Both velocities had a high Reynolds number, indicating turbulent flow. The velocity profile across the diameter was checked and was satisfactory.

2.6. Experimental Measurements

During the experimentation, the masses of sawdust collected in each element presented in Figure 2 were precisely measured and compared. The mass balance is written as the mass of incoming particles ($Mass_{feed}$) equal to the mass collected ($Mass_{coll}$) minus the losses ($loss$).

$$\Delta Mass_{feed} = Mass_{coll} - loss \quad (2)$$

The mass collected ($Mass_{coll}$) is the sum of the different collection points in the cubic box and the mass collected in the bag filter ($Mass_{bag}$) minus the losses (*loss*).

$$Mass_{feed_{ini}} - Mass_{feed_{fin}} = \sum_{Cubic\ box} Mass_{coll_i} + Mass_{bag} - loss \quad (3)$$

where $Mass_{feed_{ini}}$ corresponds to the mass of the sawdust at the beginning of the experience and $Mass_{feed_{fin}}$ corresponds to the mass of the sawdust at the end of the experiences.

The efficiency-η-of the system can be written as follows:

$$\eta = \frac{\sum_{Cubic\ box} Mass_{coll_i}}{Mass_{coll}} \quad (4)$$

The average efficiency is calculated by taking the average of the efficiencies obtained from a group of experiments having common parameters.

Experiments were performed three times or more for reasons of repeatability. Only the average values of experimentally measured quantities with small dispersion are presented.

Table 2 presents all the experimental measurements as described above and according to the criteria mentioned. Additionally, ratios are calculated, U-beam configurations are specified, and the type of sawdust is indicated.

Table 2. Experimental mass balance measurements.

Velocity	$m \cdot s^{-1}$	0.77	0.76	0.74	0.79	0.79	0.80
Mass_coll_i	g	591.47	578.25	693.52	632.3	614.29	690.93
Ratio Mass_coll_i/Mass_feed	%	69.4%	66.6%	76.0%	79.3%	84.0%	80.4%
Mass_bag	g	275.54	240.25	187.31	143.61	102.17	121.54
Ratio Mass_bag/Mass_feed	%	32.3%	27.7%	20.5%	18.0%	14.0%	14.1%
Loss	g	15.01	49.5	31.17	21.09	14.54	46.53
Ratio Loss/Mass_feed	%	1.76%	5.70%	3.42%	2.65%	1.99%	5.42%
U-Beam configuration		None	None	1 row	1 row	2 rows	2 rows
Sawdust		medium	medium	medium	medium	medium	medium
Velocity	$m \cdot s^{-1}$	0.81	0.81	0.80	0.81	0.82	1.54
Mass_feed	g	915	938	553	593	590	643
Mass_coll_i	g	748.22	757.57	432.68	420.41	422.33	241.82
Ratio Mass_coll_i/Mass_feed	%	81.8%	80.8%	78.2%	70.9%	71.6%	37.6%
Mass_bag	g	146.98	152.78	119.68	145.61	219.11	424.09
Ratio Mass_bag/Mass_feed	%	16.1%	16.3%	21.6%	24.6%	37.1%	66.0%
Loss	g	19.8	27.65	0.64	26.98	51.44	22.91
Ratio Loss/Mass_feed	%	2.16%	2.95%	0.12%	4.55%	8.72%	3.56%
U-Beam configuration		2 rows	2 rows	2 rows	2 rows	None	None
Sawdust		medium	medium	medium	medium	medium	medium
Velocity	$m \cdot s^{-1}$	1.54	1.49	1.44	1.57	1.41	1.50
Mass_feed	g	701	548	733	743	742	415
Mass_coll_i	g	336.07	351.44	418.37	408.62	412.34	198.36

Table 2. *Cont.*

Ratio Mass_coll_i/Mass_feed	%	47.9%	64.1%	57.1%	55.0%	55.6%	47.8%
Mass_bag	g	350.44	232.68	274.62	284.13	299.77	206.72
Ratio Mass_bag/Mass_feed	%	50.0%	42.5%	37.5%	38.2%	40.4%	49.8%
Loss	g	14.49	36.12	40.01	50.25	29.89	9.92
Ratio Loss/Mass_feed	%	2.07%	6.59%	5.46%	6.76%	4.03%	2.39%
U-Beam configuration		3 rows	3 rows	3 rows	3 rows	3 rows	3 rows
Sawdust		medium	medium	medium	fine	fine	fine
Velocity	$m \cdot s^{-1}$	1.43	1.44	1.51	1.39	1.45	1.34
Mass_feed	g	393.4	438	860	840	931	849
Mass_coll_i	g	178.45	214.56	487.05	539.24	580.4	694.86
Ratio Mass_coll_i/Mass_feed	%	45.4%	49.0%	56.6%	64.2%	62.3%	81.8%
Mass_bag	g	204.55	213.26	323.63	340.63	301.23	137.7
Ratio Mass_bag/Mass_feed	%	52.0%	48.7%	37.6%	40.6%	32.4%	16.2%
Loss	g	10.4	10.18	49.32	39.87	49.37	16.44
Ratio Loss/Mass_feed	%	2.64%	2.32%	5.73%	4.75%	5.30%	1.94%
U-Beam configuration		None	3 rows	3 rows	None	None	3 rows
Sawdust		fine	fine	fine	coarse	coarse	coarse
Velocity	$m \cdot s^{-1}$	1.51	1.51	1.50	1.49	1.58	1.59
Mass_feed	g	933	910	932	922	898	967
Mass_coll_i	g	699.88	707.95	687.61	683.58	675.064	756.53
Ratio Mass_coll_i/Mass_feed	%	75.0%	77.8%	73.8%	74.1%	75.2%	78.2%
Mass_bag	g	173.16	176.34	189.53	212.29	198.71	209.22
Ratio Mass_bag/Mass_feed	%	18.6%	19.4%	20.3%	23.0%	22.1%	21.6%
Loss	g	59.96	25.71	54.86	26.13	24.226	1.25
Ratio Loss/Mass_feed	%	6.43%	2.83%	5.89%	2.83%	2.70%	0.13%
U-Beam configuration		3 rows	3 rows	2 rows	2 rows	4 rows	4 rows
Sawdust		coarse	coarse	coarse	coarse	coarse	coarse

2.7. Computational Fluid Dynamics

A computational fluid dynamics (CFD) study was performed to compare experimental measurements to computational simulations. In turbulence situation, the standard k-ε model was selected to calculate the continuity equations and Reynolds-Averaged Navier Stokes equations (RANS), as reported by authors [41]. In addition, a meshing of the horizontal plane of the impactor system was carried out on two versions—one with two rows of impactors and another with three.

COMSOL Multiphysics was employed to model, simulate, and visualize flow velocities within an impactor system. A no-slip condition was applied at the boundaries. Particle representation was omitted to reduce model complexity. The case study represents only two or three rows of four U-beams.

3. Results and Discussion

The losses in all tests represent less than 7% of the mass collected. Moreover, all particles were measured using a precise balancer accurate to 0.1%, ensuring the precision and accuracy of our measurements for all tests.

The velocity of the flow, granulometry of the particles, and arrangement of the rows have significant effects on the separation efficiency of the separator. The results are presented to demonstrate the impact of these parameters on the device.

3.1. Effect of the Velocity

The velocity parameter is the key to designing the system. If it is too slow, the particles may not reach the bag filter and the system would be ineffective.

If the velocity is too high, the particles that were initially stopped by the U-beam could be reintroduced into the flow. Figure 7 shows the average efficiency of the system with or without the U-beam at different velocities. At higher velocities, fewer particles fall in the empty system, but with the U-beam, there is more particle entrainment, even though precautions have been taken to limit these effects. The velocity chosen in this study corresponds to the velocity in the fluidized bed, which is equal to 1.5 $m \cdot s^{-1}$ at the zone with U-beams.

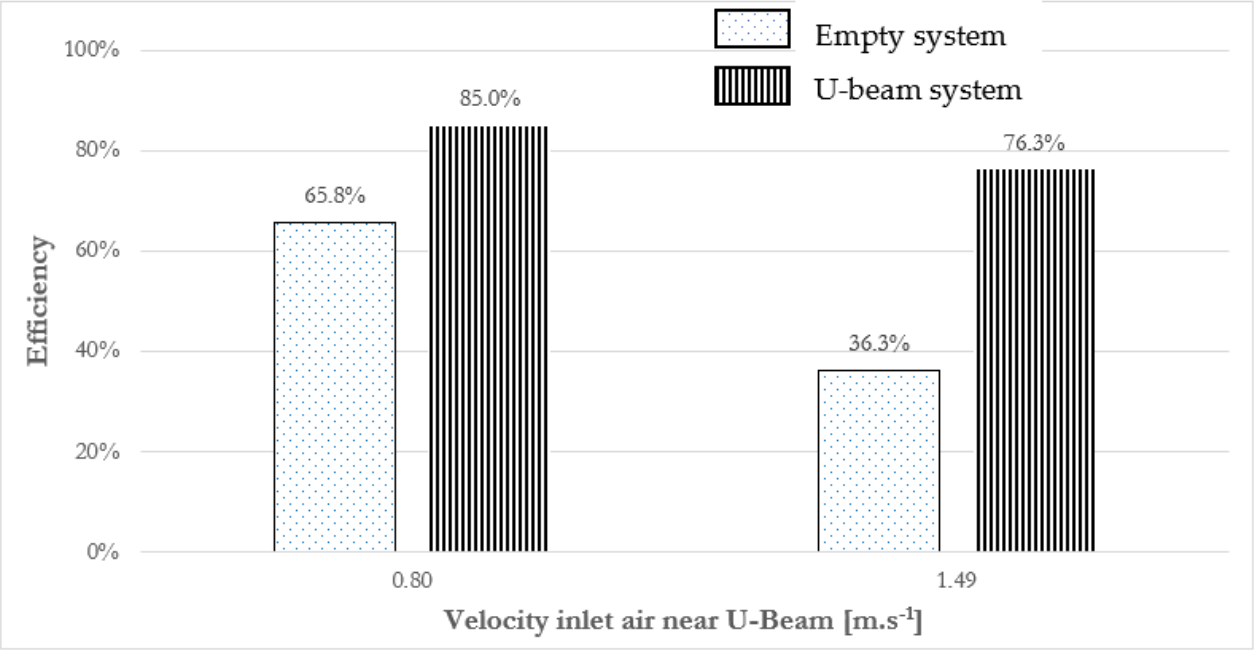

Figure 7. Average efficiency of the system (empty or with the U-beam) in function of the initial velocity inlet air.

The effect of velocity on the efficiency of separation is a compromise between the suspension velocity of the particle and the gas velocity. Firstly, the particles become more separable from the flow due to their increased inertia. However, with higher gas velocity, the entrainment capacity is greater. This phenomenon was also observed in studies conducted by the authors in [14,42]. Even though the efficiency is lower at high speed with the U-beam, the relative efficiency of the U-beam is twice as good as that at lower speed. As the authors suggested an optimized efficiency around 4 $m \cdot s^{-1}$, we could expect to find better results at a higher speed.

3.2. Effect of the Granulometry

The maximum efficiency of the system is achieved with coarse particles, as shown in Figure 8. According to [43], for particles larger than 3 µm, the drag force is lower than the

centrifugal force, meaning that the main separation phenomenon in our case is the change in flow direction between the solid and the gas.

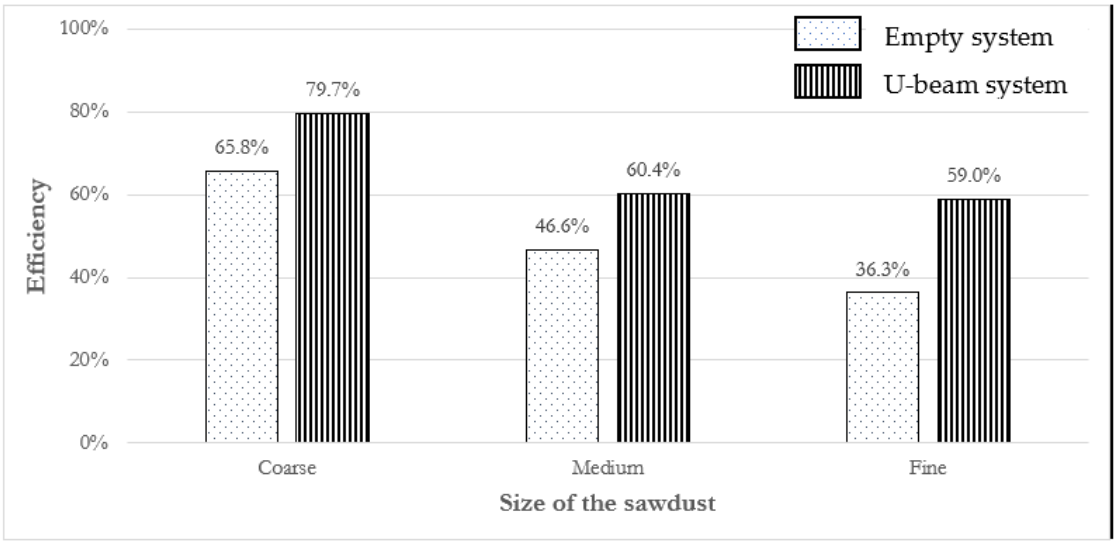

Figure 8. Efficiency of the system (empty or with the U-beam) in function of the size of the sawdust.

However, when considering the impact of the empty system, the relative efficiency of rows is 14% for coarse and medium particles and 23% for fine particles.

The system becomes less efficient as the particles become finer, with efficiency decreasing by half between coarse and fine particles.

In all three types of granulometry, the U-beam system is more effective at trapping particles than the empty system. This means that the U-beam system is able to mitigate the issue of particles flying away, albeit with varying degrees of efficiency. In particular, it was observed that the flying away of particles was more prominent for fine particle sizes (as shown in Figures 8 and 9). As noted by [25], the U-beam device has little impact on the efficiency for medium-sized particles.

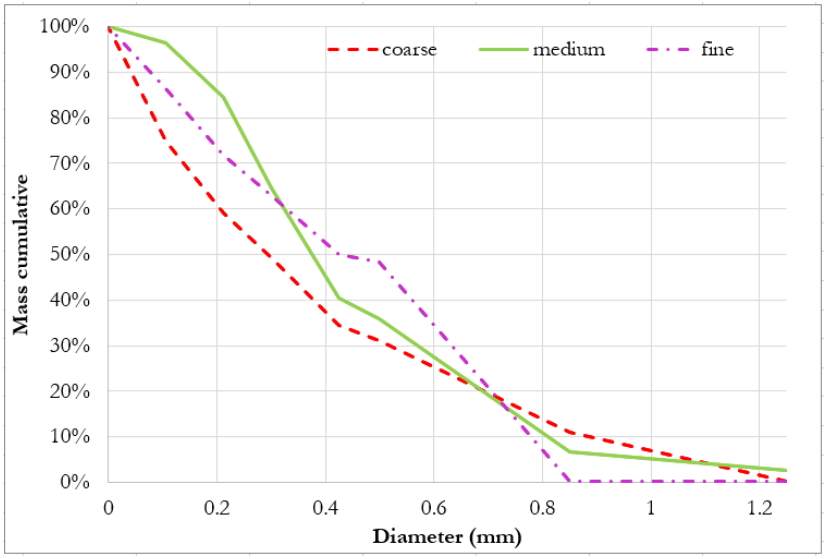

(**a**)

Figure 9. *Cont.*

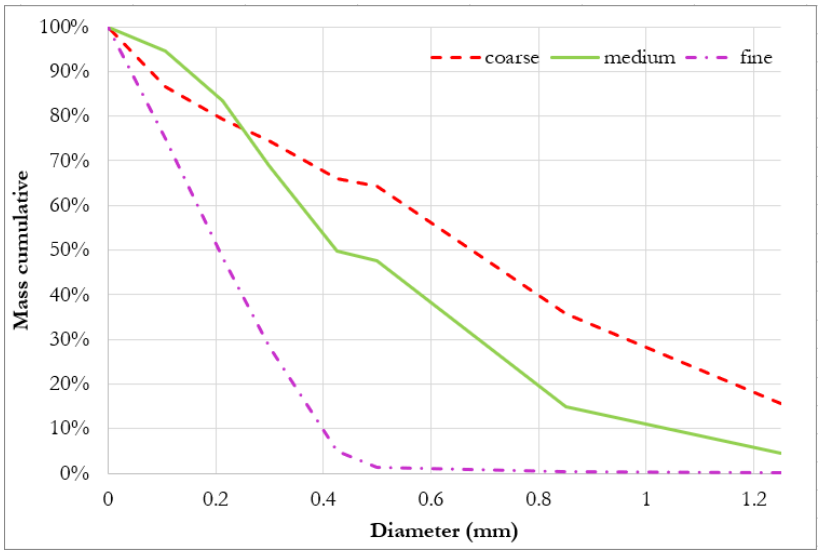

(**b**)

Figure 9. Granulometry in bag filter for three rows 2,3,4 (**a**), empty (**b**).

Particles from all three types of sawdust were collected both during empty (Figure 9b) tests and U-beam (Figure 9a) tests in the bag filter.

These particles were subjected to particle size tests to determine which sizes were stopped by the system.

In Figure 9, the medium particles have a similar distribution for both graphs. Coarse particles are stopped better by the three-row U-beam system than by the empty system because the flying away phenomenon cannot transport coarse or heavy particles. However, fine particles are more challenging to stop. In the empty system, no particles with a diameter greater than 0.5 mm were found, whereas in the case of the U-beam system, this value increased to 0.8 mm.

The U-beam system was able to stop more than 10% of particles greater than 1 mm and around 3% of particles greater than 1.25 mm.

To compare the three granulometries, Figure 10 shows the difference between the results of Figure 9 for each particle size. Indeed, we subtracted the quantities of particles obtained in the empty system from those in the system with three rows. For fine particles, the flying away phenomenon is well represented for particles with sizes larger than 0.5 mm, while most fine particles are around 0.3 mm.

For the medium particle size, the system with impactors was more effective in stopping particles larger than 0.5 mm, which corresponds to the average particle size in this category. For coarse particles with sizes greater than 1.25 mm, the trapping efficiency was effective on all particle sizes at over 10% compared to the empty system.

3.3. Effect of the Geometry of the Separator

It is important that the particle fallout area is not in contact with the flow. Systems with barriers between the flow and the stopped particles can also be considered but this is more difficult. Flying away can occur.

During tests, the number of each row changed as mentioned earlier. The number of each row indicated in the results are the same as in Figure 4. Each test with a different configuration was recorded by the row number. The same tests were put together to create average data. In Figure 11, four categories of configurations show the efficiency of the system according to the configuration of the U-beam.

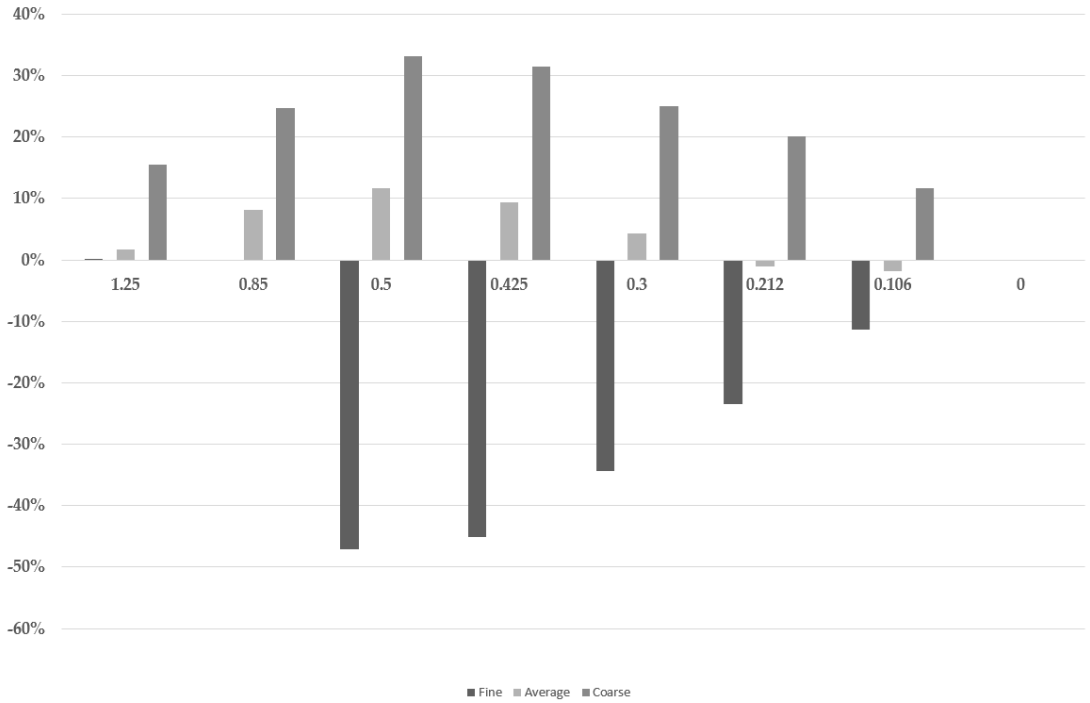

Figure 10. Difference between the granulometry found in bag filter for three rows and the granulometry found in bag filter with an empty system.

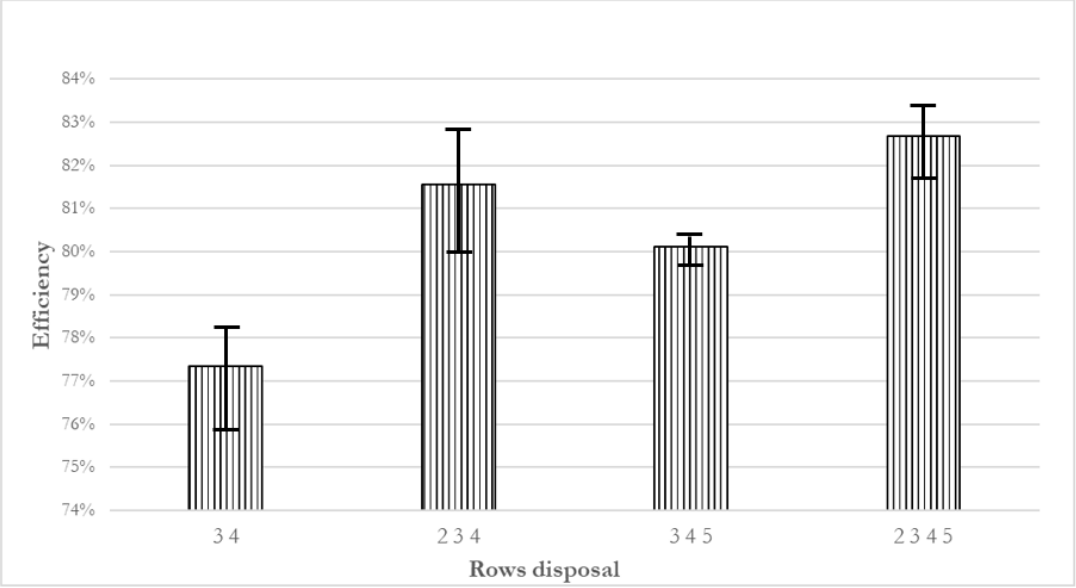

Figure 11. Efficiency of the system in function of the rows disposal U-beam for V = 1.5 m·s^{-1}.

According to Table 2, the average efficiency of the empty system is 64%.

The histograms in Figure 11, labelled 2,3,4 and 3,4,5, correspond to experiments conducted with three rows of impactors. The difference between the two experiments is the position of the rows (see Figure 4). Regarding the dispersion of the results, in the first case, the flow has less time to stabilize before encountering the impactors. The efficiency is higher, but the measurement dispersion is greater. The difference between the two configurations is not significant enough to establish a general design rule.

One row did not yield any significant results and was not included in Figure 11. Adding two rows in the middle of the box resulted in an increase in efficiency of more

than 10%, while adding another row directly next to the first two rows resulted in a 3.5% increase in efficiency. The addition of a fourth row resulted in less than a 2% increase in efficiency, which may not be worth the technical and financial effort required.

These results were compared to the results presented by [14], who conducted similar tests. The efficiency curve of the impactor used by those authors was similar to ours and was 80% for three rows and 85–90% for four rows. The authors suggested that the best efficiency was achieved at a velocity of 4 $m \cdot s^{-1}$, which was higher than that used in our study. The difference in results could be explained by the influence of velocity.

Our results were also compared to the design of the inertial impaction of the CFB and validated the solution of having two areas of U-beam series [20]. Adding rows to the device does not proportionally increase the efficiency of the system, but choosing two U-beam zones with different cut-off diameters can increase efficiency.

3.4. Modeling Checking

Modelling of the two-row and three-row versions shows the difference in local pressure around the U-beam in the two configurations (Figure 12). The local pressure is higher in the three-row configuration, which means that the effect of the centrifugal force applied to the particle is greater in this configuration. Trapping efficiency is enhanced when the particle is forced out of the gas stream. The inlet velocity is equal to 1.5 $m \cdot s^{-1}$ in this case and the flow rate is equal to 300 m^3/h.

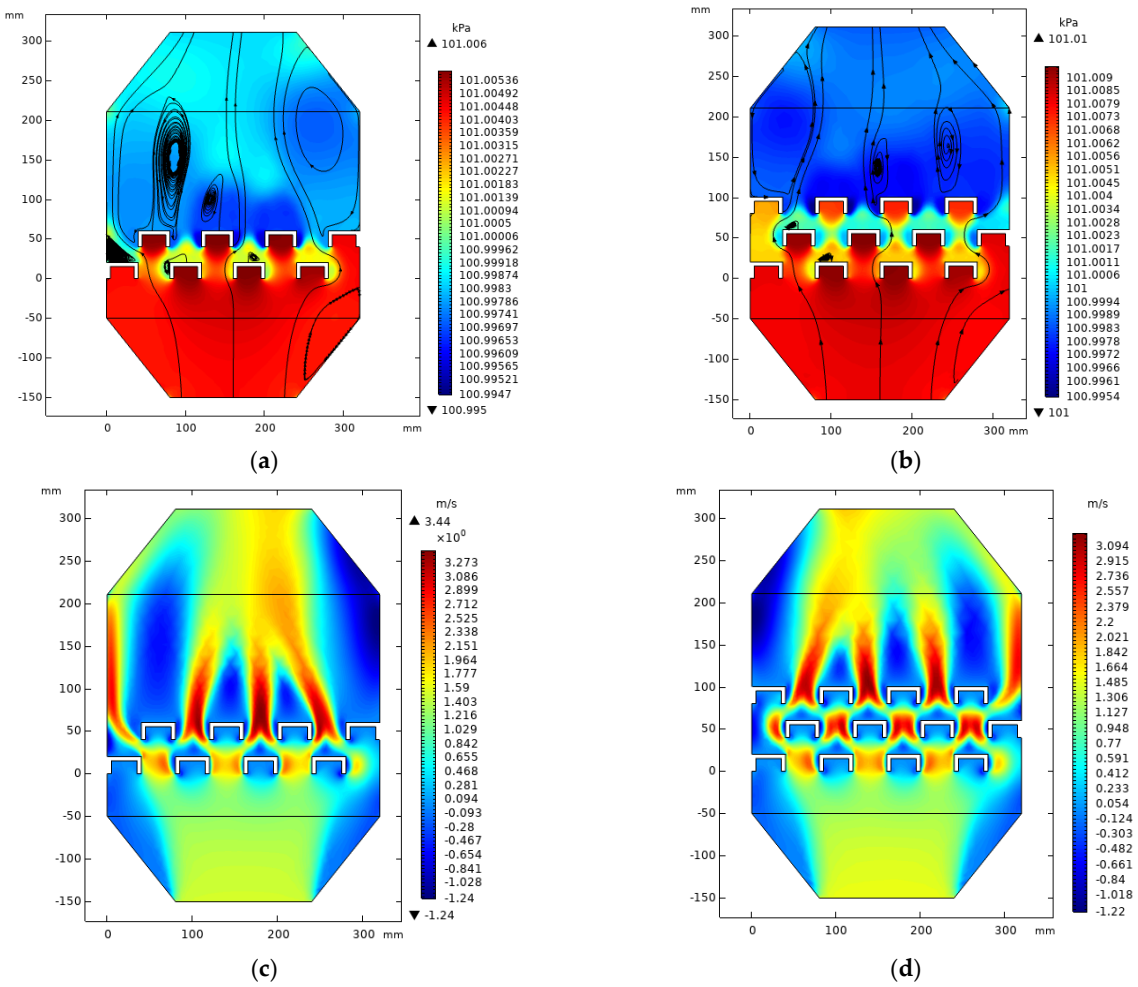

Figure 12. Two-dimensional modeling of air flow through 2 rows (**a**–**c**) and 3 rows (**b**–**d**). Pressure results (**a**,**b**) and velocity results (**c**,**d**).

The results of the flow curve, especially for Figure 12b, are quite similar to the former CFD analysis [38].

The influence of the addition of a row is measurable in the simulation by a greater difference in the pressures upstream and downstream of the impactor system, and also on velocity pictures (Figure 12c,d), where the speed is increasing between the U-beams. Finally, from these figures, the side effects and the importance of effective sealing can be understood.

4. Conclusions

The efficiency of the U-beam technology was tested and found to be effective in trapping particles, even fine ones, making it a cost-effective and viable alternative to the cyclone as a fluidized bed boiler. The following summarizes the key findings of the study:

The efficiency of the impactor is around 80% for three rows and 85–90% for four rows. The U-beam device can be used as a pretreatment for dusty systems with a cut-off diameter of 1.25 mm, effectively trapping a significant amount of fine particles. This allows for a smaller MDC or adjustment to the cut-off diameter.

The system's overall performance can be increased by up to 15% by selecting the best combination of U-beams. Three rows of U-beams are ideal for a Reynolds numbers (2.10^5), while two rows are sufficient for a lower Reynolds numbers (1.10^5).

The design rules for the arrangement of the U-beam system are as follows:

- A minimum of two rows (maximum four) covering the entire surface normal to the flow;
- A space between two rows equal to one time of the width of the U-beam;
- Attention given to sealing and optimizing the airflow;
- The system of U-beams should be designed to limit particle flight and allow for easy removal to maintain the impactor system's efficiency.

Author Contributions: Writing—original draft preparation, R.A.; materials and investigation, R.A., M.D. and S.A.; analysis, R.A., M.D. and Y.R.; review and supervision, Y.R. All authors have read and agreed to the published version of the manuscript.

Funding: LERMAB is supported by a grant overseen by the French National Research Agency (ANR) as part of the "Investissements d'Avenir" program (ANR-11-LABX-0002-01. Lab of Excellence ARBRE) and is part of ICEEL.

Data Availability Statement: Data sharing not applicable.

Conflicts of Interest: The authors declare no conflict of interest.

Nomenclature

CFB	Circulating fluidized bed
D	Inner diameter (m)—9.4×10^{-2}
IPCC	Intergovernmental Panel on Climate Change
Loss	the loss of sawdust mass collected
MDC	Mechanical dust collector
$\boldsymbol{Mass_{feed_{ini}}}$	Initial mass of the feeding system for the sawdust (g)
$\boldsymbol{Mass_{feed_{fin}}}$	Final mass of the feeding system for the sawdust (g)
$\boldsymbol{Mass_{coll_i}}$	Mass collected in the entire system (g)
$\boldsymbol{Mass_{bag}}$	Mass collected in the bag (g)
MWth	Thermal megawatt (MW)
RANS	Reynolds-Averaged Navier Stokes equations
Re	Reynolds number
RDF	Refuse-Derived Fuels
SRF	Solid Recovery Fuels

UPN	Steel beam in «U» shape conforming to the EN 10365 standard and EN 10279 for tolerances
V	Velocity of the air flow ($m \cdot s^{-1}$)
Greek letters	
η	Efficiency
ρ	Density ($kg \cdot m^{-3}$) 1.204 for air at 20 °C under 1.013×10^5 Pa
μ	Dynamic viscosity ($kg \cdot (m \cdot s)^{-1}$ 1.8×10^{-5}

References

1. IPCC. Global Warming of 1.5 °C. 2022. Available online: https://www.ipcc.ch/sr15/ (accessed on 6 October 2022).
2. Van Loo, S.; Kopperjan, J. *The Handbook of Biomass Combustion & Co-Firing*; Earthscan: London, UK, 2008. [CrossRef]
3. Johansen, K. A Brief History of District Heating and Combined Heat and Power in Denmark: Promoting Energy Efficiency, Fuel Diversification, and Energy Flexibility. *Energies* **2022**, *15*, 9281. [CrossRef]
4. Koornneef, J.; Junginger, M.; Faaij, A. Development of fluidized bed combustion—An overview of trends, performance and cost. *Prog. Energy Combust. Sci.* **2007**, *33*, 19–55. [CrossRef]
5. Odzijewicz, I.J.; Wołejko, E.; Wydro, U.; Wasil, M.; Jabłońska-Trypuć, A. Utilization of Ashes from Biomass Combustion. *Energies* **2022**, *15*, 9653. [CrossRef]
6. Boriouchkine, A.; Zakharov, A.; Jämsä-Jounela, S.-L. Dynamic modeling of combustion in a BioGrate furnace: The effect of operation parameters on biomass firing. *Chem. Eng. Sci.* **2012**, *69*, 669–678. [CrossRef]
7. Bicocchi, S.; Boulinguez, M.; Diard, K. *Les Polluants et Les Techniques D'épuration des Fumées*; RECORD; Lavoisier: Paris, France, 2009. Available online: https://www.lavoisier.fr/livre/environnement/les-polluants-et-les-techniques-d-epuration-des-fumees-2-ed/bicocchi/descriptif-9782743011901 (accessed on 26 June 2023).
8. Altmeyer, S.; Mathieu, V.; Jullermier, S.; Contral, P.; Midoux, N.; Rode, S.; Leclerc, J.P. Comparison of different models of cyclone prediction performance for various operating conditions using a general software. *Chem. Eng. Process. Process Intensif.* **2004**, *43*, 511–522. [CrossRef]
9. Ganegama Bogodage, S.; Leung, A.Y.T. CFD simulation of cyclone separators to reduce air pollution. *Powder Technol.* **2015**, *286*, 488–506. [CrossRef]
10. Alves, A.; Paiva, J.; Salcedo, R. Cyclone optimization including particle clustering. *Powder Technol.* **2015**, *272*, 14–22. [CrossRef]
11. Wan, G.; Sun, G.; Xue, X.; Shi, M. Solids concentration simulation of different size particles in a cyclone separator. *Powder Technol.* **2008**, *183*, 94–104. [CrossRef]
12. Szyszlak-Bargłowicz, J.; Wasilewski, J.; Zając, G.; Kuranc, A.; Koniuszy, A.; Hawrot-Paw, M. Evaluation of Particulate Matter (PM) Emissions from Combustion of Selected Types of Rapeseed Biofuels. *Energies* **2023**, *16*, 239. [CrossRef]
13. Khan, A.A.; de Jong, W.; Jansens, P.J.; Spliethoff, H. Biomass combustion in fluidized bed boilers: Potential problems and remedies. *Fuel Process Technol.* **2009**, *90*, 21–50. [CrossRef]
14. Kefa, C.; Li, X.; Li, Y.; Yan, J.; Shen, Y.; Liang, S.; Ni, M. Experimental study of a finned tubes impact gas-solid separator for CFB boilers. *Chem. Eng. J.* **1997**, *66*, 159–169. [CrossRef]
15. Zhu, Q. Developments in Circulating Fluidised Bed Combustion. IEA Clean Coal Center. 2013. Available online: https://usea.org/sites/default/files/042013_Developments%20in%20circulating%20fluidised%20bed%20combustion_ccc219.pdf (accessed on 26 June 2023).
16. Leckner, B. Hundred years of fluidization for the conversion of solid fuels. *Powder Technol.* **2022**, *411*, 117935. [CrossRef]
17. Belin, F.; Walker, D.J. Impingement Type Solids Collector Discharge Restrictor. U.S. Patent 4,891,052, 2 January 1990. Available online: https://patents.google.com/patent/US4891052 (accessed on 26 June 2023).
18. Belin, F.; James, D.E.; Walker, D.J. Internal Impact Type Particle Separator. U.S. Patent 4,992,085, 12 February 1991. Available online: https://patents.google.com/patent/US4992085A (accessed on 26 June 2023).
19. Daum, E.D.; Rowley, D.R. Water/Steam-Cooled U-Beam Impact Type Particle Separator. U.S. Patent 5,435,820, 25 July 1995. Available online: https://patents.google.com/patent/US5435820 (accessed on 26 June 2023).
20. James, D.E.; Walker, D.J.; Belin, F. Indirect Cooling of Primary Impact Type Solids Separator Elements in a CFB Reactor. U.S. Patent 5,809,940, 22 September 1998. Available online: https://patents.google.com/patent/US5809940 (accessed on 26 June 2023).
21. Walker, D.J. Particulate Collector Channel with Cooling Inner Elements in a CFB Boiler. U.S. Patent 6322603B1, 27 November 2001. Available online: https://patents.google.com/patent/US6322603B1 (accessed on 26 June 2023).
22. Maryamchik, M.; Alexander, C.K.; Belin, F.; Gibbs, D.R.; Walker, D.J.; Wietzke, D.L. CFB impact type particle collection elements attached to cooled supports. U.S. Patent 6454824B1, 24 September 2002. Available online: https://patents.google.com/patent/US6454824B1/en (accessed on 6 October 2002).
23. Basu, P.; Fraser, S.A. Chapter 7—Gas-solid separators. In *Circulating Fluidized Bed Boilers*; Basu, P., Fraser, S.A., Eds.; Butterworth-Heinemann: Oxford, UK, 1991; pp. 201–228. [CrossRef]
24. Belin, F.; Walker, J.D. Drainable Discharge Pan for Impact Type Particle Separator. U.S. Patent 5799593A, 1 September 1998. Available online: https://patents.google.com/patent/US5799593A/en (accessed on 6 October 2022).
25. De, S.; Nag, P.K. Pressure drop and collection efficiency of cyclone and impact separators in a CFB. *Int. J. Energy Res.* **1999**, *23*, 51–60. [CrossRef]

26. Basu, P. Combustion of coal in circulating fluidized-bed boilers: A review. *Chem. Eng. Sci.* **1999**, *54*, 5547–5557. [CrossRef]
27. ADEME. Référentiels Combustibles Bois Energie de l'ADEME. Définition et Exigences. 2017. Available online: https://librairie.ademe.fr/energies-renouvelables-reseaux-et-stockage/1783-referentiels-combustibles-bois-energie-de-l-ademe.html (accessed on 2 December 2022).
28. ADEME. Biomasse Energie et Produits Biosourcés. Recueil de Projets Soutenus Par l'ADEME Entre 2008 et 2015, 8744, 2016. Available online: https://librairie.ademe.fr/energies-renouvelables-reseaux-et-stockage/2321-biomasse-energie-et-produits-biosources-9791029703386.html (accessed on 6 October 2022).
29. Anantharaman, A.; Cocco, R.A.; Chew, J.W. Evaluation of correlations for minimum fluidization velocity (Umf) in gas-solid fluidization. *Powder Technol.* **2018**, *323*, 454–485. [CrossRef]
30. Wen-Ching, Y. *Handbook of Fluidization and Fluid-Particle Systems*; Marcel Dekker: New York, NY, USA, 2003. [CrossRef]
31. Morris, J.D.; Daood, S.S.; Chilton, S.; Nimmo, W. Mechanisms and mitigation of agglomeration during fluidized bed combustion of biomass: A review. *Fuel* **2018**, *230*, 452–473. [CrossRef]
32. Anicic, B.; Lin, W.; Dam-Johansen, K.; Wu, H. Agglomeration mechanism in biomass fluidized bed combustion—Reaction between potassium carbonate and silica sand. *Fuel Process. Technol.* **2018**, *173*, 182–190. [CrossRef]
33. Aubry, R.; Préau, S.; Martin, G.; Brenot, P.; Chobaut, J.-P.; Rogaume, Y. Projet POLYBIOM. 2018. Available online: https://icar-cm2t.com/wp-content/uploads/2020/11/Synthese-POLYBIOM-dossier-Ademe.pdf (accessed on 11 October 2022).
34. Winaya, N.S.; Basu, P.; Reddy, B.V. Experimental investigations on heat transfer from suspension to impact separators in the riser column of a circulating fluidized bed combustor. *Int. J. Heat Mass Transf.* **2003**, *46*, 71–75. [CrossRef]
35. Adamczyk, W.P.; Kozolub, P.; Kruczek, G.; Pilorz, M.; Klimanek, A.; Czakiert, T.; Wecel, G. Numerical approach for modeling particle transport phenomena in a closed loop of a circulating fluidized bed. *Particuology* **2016**, *29*, 69–79. [CrossRef]
36. Wischnewski, R.; Ratschow, L.; Hartge, E.-U.; Werther, J. Reactive gas–solids flows in large volumes—3D modeling of industrial circulating fluidized bed combustors. *Particuology* **2010**, *8*, 67–77. [CrossRef]
37. Shah, S.; Myöhänen, K.; Kallio, S.; Hyppänen, T. CFD simulations of gas–solid flow in an industrial-scale circulating fluidized bed furnace using subgrid-scale drag models. *Particuology* **2015**, *18*, 66–75. [CrossRef]
38. Baskakov, A.P.; Mudrechenko, A.V.; Bubenchikov, A.M.; Starchenko, A.V.; Gogolev, A.F.; Markovich, D.M. Modeling of U-beam separator. *Powder Technol.* **2000**, *107*, 84–92. [CrossRef]
39. Zevenhoven-Onderwater, M. Ash-Forming Matter in Biomass Fuels. Ph.D. Thesis, Faculty of Engineering, Process Chemestry Group Abo Akademi, Turku, Finland, 2001. Available online: http://users.abo.fi/mzevenho/portfolj/publikationer/PhD%20MZ.pdf (accessed on 26 June 2023).
40. Obernberger, I.; Brunner, T.; Jöller, M. Characterisation and formation of aerosols and fly-ashes from fixed bed biomass combustion. In Proceedings of the IEA-Seminar Aerosols from Biomass Combustion, Zurich, Switzerland, 27 June 2001; pp. 66–74.
41. Promtong, M.; Phirommark, P.; Suvanjumrat, C.; Chookaew, W.; Uapipatanakul, S. A CFD Study of Particle Flows (PM1, PM10, PM100) in Lowvolume Impact Separator. *Geomate J.* **2022**, *22*, 53–61. [CrossRef]
42. Hamelin, J.P.M.; Basu, P.; Hamdullahpur, F. A study into the operation of an impact-type gas–solid separator. *Int. J. Energy Res.* **2004**, *28*, 1023–1032. [CrossRef]
43. Song, C.; Pei, B.; Jiang, M.; Wang, B.; Xu, D.; Chen, Y. Numerical analysis of forces exerted on particles in cyclone separators. *Powder Technol.* **2016**, *294*, 437–448. [CrossRef]